THE JOURNAL OF PHYSICAL CHEMISTRY C

ARTICLE

pubs.acs.org/JPCC

Investigation of the Transition Voltage Spectra of Molecular Junctions Considering Frontier Molecular Orbitals and the Asymmetric Coupling Effect

Gunuk Wang,[†] Yonghun Kim,[†] Seok-In Na,[§] Yung Ho Kahng,[∥] Jamin Ku,[†] Sungjun Park,[†] Yun Hee Jang,[†] Dong-Yu Kim,[†,‡] and Takhee Lee*[,†,‡,⊥]

[†]School of Materials Science and Engineering and [‡]WCU Department of Nanobio Materials and Electronics, Gwangju Institute of Science and Technology, Gwangju 500-712, Korea

[§]Korea Institute of Science and Technology, Institute of Advanced Composite Materials, Jeollabuk-do, 565-902, Korea

[∥]Research Institute for Solar and Sustainable Energies, Gwangju Institute of Science and Technology, Gwangju 500-712, Korea

Supporting Information

ABSTRACT: This study experimentally and theoretically investigated the characteristics of transition voltage spectroscopy (TVS) with different asymmetric coupling in molecular junctions that were formed by several alkyl- and oligoacene-based molecules. On the basis of the analysis of a statistically significant number of device data (a total of ~300 devices and ~880 TVS data), we confirmed that the minimum point appearing in the Fowler−Nordheim (F−N) plot of the current−voltage characteristics depended linearly on the energy offset between the Fermi energy of the electrodes and the highest-occupied molecular orbital (HOMO) energy level of the molecular channel. We also observed that the slope of the log(I)−log(V) plot in molecular junctions changed sequentially. In addition, we extended a coherent molecular model by considering both the HOMO and the lowest-unoccupied molecular orbital (LUMO) levels of molecules and developed more comprehensive explanations for the TVS characteristics that are influenced by the asymmetric coupling, molecular length, and molecular orbital as well as for the sequential change in the slope of the log(I)−log(V) plot in molecular junctions.

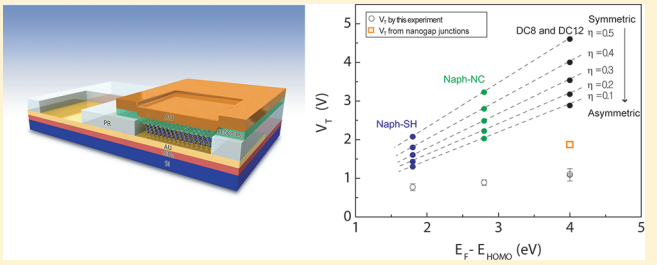

INTRODUCTION

A general prerequisite for developing molecular electronic devices is a comprehensive understanding of the relation between the molecular orbitals and the electronic transport properties of molecular junctions.[1−3] In molecular electronic junctions, the frontier orbitals (i.e., the highest-occupied molecular orbital (HOMO) and the lowest-unoccupied molecular orbital (LUMO)) of the molecules with respect to the Fermi level of the electrodes are important factors for electronic transport properties.[1−5] The difference between the energy levels of the HOMO or LUMO (E_{HOMO} or E_{LUMO}) from the Fermi energy level (E_F), that is, $|E_F - (E_{HOMO}$ or $E_{LUMO})|$, determines the barrier height,[6,7] which sets the different conducting criteria for molecular junctions.[3,5,8] In 2006, Beebe et al. found a creative and simple method to estimate the barrier heights in molecular junctions. They observed that on metal−molecule−metal junctions with π-conjugated thiols of small HOMO−LUMO gaps the current−voltage (I−V) curves showed a transition from direct tunneling (DT) to field emission, which is known as Fowler−Nordheim (F−N) tunneling.[6] The authors estimated the position of the nearest molecular orbital level with respect to the Fermi level of the electrodes, which determines the tunneling barrier height using a transition voltage (V_T) profile from DT to F−N tunneling. This technique, which is called transition voltage spectroscopy (TVS), possesses the advantage of omitting the temperature-variable apparatus, and TVS can also be utilized as a good tool for obtaining barrier heights. Another main advantage of TVS is that one can study molecular junctions before the breakdown. The molecular junction often becomes unstable and breaks down because of the large current density and huge electric field when a large enough voltage is applied to probe HOMO or LUMO resonances. However, in TVS characterization, the TVS peaks (corresponding to the tails of HOMO or LUMO resonances) are obtained at relatively low voltage before the breakdown.[9−11] Consequently, the TVS technique has been applied to various molecular junctions[3,6,7,12−15] and even to semiconductor devices to obtain the barrier height.[16]

However, several interesting questions about TVS have been raised. For example, the TVS results for certain molecular junctions, such as alkanethiol junctions, showed

Received: May 10, 2011
Revised: August 7, 2011
Published: August 24, 2011

molecular-length-independent transition voltage properties.[6] This phenomenon cannot be described within the framework of the conventional model (i.e., the Simmons tunneling model).[3,6,7,17] Later, these confusing results were resolved by Huisman et al. with a coherent molecular model that considered the HOMO level of alkyl molecules based on the Lorentzian-based transmission function. The model theoretically predicted that the transition voltage in alkyl-based molecular junctions was independent of the molecular length, except in cases of short molecules (particularly shorter than ~9 Å).[10]

Recently, another theoretical paper on TVS reported that the minimum point in the F−N plot is one of the general features in the integration of the tail of bell-shaped functions such as Lorentzian and Gaussian functions.[11] This means that the minimum point does not necessarily correspond to the voltage for the exact onset of resonant tunneling. Furthermore, Chen et al. reported that the value of $(E_F - E_{HOMO})/V_T$ was found to vary from 0.86 to 2.0, depending on the junction asymmetry; this value is based on extensive ab initio calculations of the nonlinear current−voltage relations for a broad class of molecular junctions.[18]

However, in view of the importance of the TVS technique in understanding molecular or organic electronic devices, more experimental and theoretical analyses on TVS are required. For example, to date, the research on the TVS of molecular junctions have been done mainly by conducting atomic force microscopy (CAFM) and cross-wires junction techniques.[6,7,12−14] However, in terms of device applications, solid-state device structure is more preferable to CAFM or cross-wires junction testbeds. Furthermore, in CAFM or cross-wires junction tools, it is not trivial to perform temperature-variable electrical characterizations to investigate charge conduction mechanisms to rule out parasitic transport mechanisms other than the tunneling transport mechanism unambiguously such as thermionic or defects-mediated transports. It is necessary to statistically analyze the TVS properties because the statistical approach is critically important for truly understanding the molecular charge transport characteristics and for reliable device applications. Also, the influence of the frontier molecular orbitals (i.e., HOMO and LUMO levels), molecular contacts, molecular structures, and the asymmetric coupling on TVS characteristics needs to be further theoretically investigated.

In this study, we report the statistical analysis of a large quantity of TVS data (a total of 883 TVS data) acquired from asymmetric metal−molecule−metal junctions (i.e., Au/SAM/PEDOT:PSS). Two prototypes of molecules, alkyl- and oligoacene-based molecules, were used in this study. Molecules with various lengths and contact groups were chosen to investigate the effects of these factors on the TVS characteristics and the change in transport regimes. Additionally, we extended the coherent molecular model by considering both the HOMO and LUMO levels of the molecules under different coupling strengths to the electrodes. We also developed more comprehensive explanations for the TVS characteristics that are influenced by asymmetric coupling, molecular length, and molecular orbital as well as for the sequential change in the slope of the $\log(I)-\log(V)$ plot in molecular junctions.

EXPERIMENTAL SECTION

Device Fabrication. A conventional photolithography method was used to pattern the bottom electrodes with Au (150 nm) and Ti (5 nm) on a p-type (100) Si substrate covered with thermally grown 300 nm thick SiO_2 in an electron beam evaporator under a pressure of $\sim 10^{-7}$ Torr and with a very low deposition rate of 0.1 to 0.2 Å. The root-mean-square (rms) roughness for the Au bottom electrode was found to be 0.7 to 0.8 Å using atomic force microscopy (AFM) images with a scan size of $2\,\mu m \times 2\,\mu m$ (data not shown). Then, a positive photoresistor (PR) (AZ6612) was spin-coated on top of the Au bottom electrodes to isolate the molecular junctions electrically. The junctions were square-shaped with side lengths of 40 and 90 μm. After the isolation process, the devices with PR patterns were annealed for at least 1 h at a temperature of 474 K to make the PR insoluble in ethanol during the formation of self-assembled monolayers (SAMs) on the electrode. The SAMs were formed on the Au bottom electrode in a nitrogen-filled glovebox with an oxygen level of less than ~10 ppm for 1 to 2 days. Then, the devices were thoroughly rinsed with ethanol to remove the remaining unbound molecules. On top of the SAMs, a suspension of conducting polymer PEDOT:PSS (poly-(3,4-ethylenedioxythiophene) stabilized with poly-(4-styrenesulfonic acid)) was spin-coated in two steps. The first step was at 500 rpm for 5 s, and the second step was at 3000 rpm for 35 s. The electrically conductive PEDOT:PSS layer prevented the formation of electrical shorts upon deposition of the Au top electrode. The thickness of the PEDOT:PSS layer was found to be 200 to 300 nm and was measured by a surface profiler (Kosaka ET-3000i). We added dimethyl sulfoxide (DMSO) to PEDOT:PSS (from H. C. Starck), which is a highly doped polymer with a conductivity of $\sim 300\ S \cdot cm^{-1}$ obtained by a standard four-point-probe system with a Keithley 2400 current source and a HP 34420A nanovoltmeter. To avoid the unexpected thermal deterioration of the SAMs, we dried the devices coated with PEDOT:PSS at room temperature in a vacuum of $\sim 1 \times 10^{-3}$ Torr.

Then, the Au top electrode (thickness 50−100 nm) was deposited on top of the PEDOT:PSS layer using an electron beam evaporator through a shadow mask. Reactive ion etching (RIE) with O_2 was used to remove the redundant PEDOT:PSS. The Au top electrode was used as a contact with the probes and as a shadow mask, whereas PEDOT:PSS was etched away using RIE to prevent a direct current path through PEDOT:PSS from Au top electrodes to Au bottom electrodes. All $I-V$ curves were obtained with a biasing condition that the voltage is applied to the top electrode (PEDOT:PSS/Au) while the bottom electrode (Au) is grounded.

Formation of Self-Assembled Monolayer. Four molecular species (DC8, DC12, Naph-NC, and Naph-SH) were self-assembled from molecular solutions on Au bottom electrodes. For molecular deposition, we used 5 mM molecular solutions and an incubation time of 1 to 2 days in a nitrogen-filled glovebox with an oxygen level of less than ~10 ppm to avoid potential oxidation problems.

RESULTS AND DISCUSSION

Figure 1 shows a series of scanning electron microscope (SEM) images of fabricated metal−molecule−metal junctions devices (Figure 1a), including a schematic diagram of the molecular junction (Figure 1b). To prevent the penetration of the top metal electrode, which could have caused an electrical short, we inserted an interlayer of high-conducting polymer (poly-(3,4-ethylenedioxythiophene) stabilized with poly-(4-styrenesulfonic acid), which is denoted by PEDOT:PSS) between

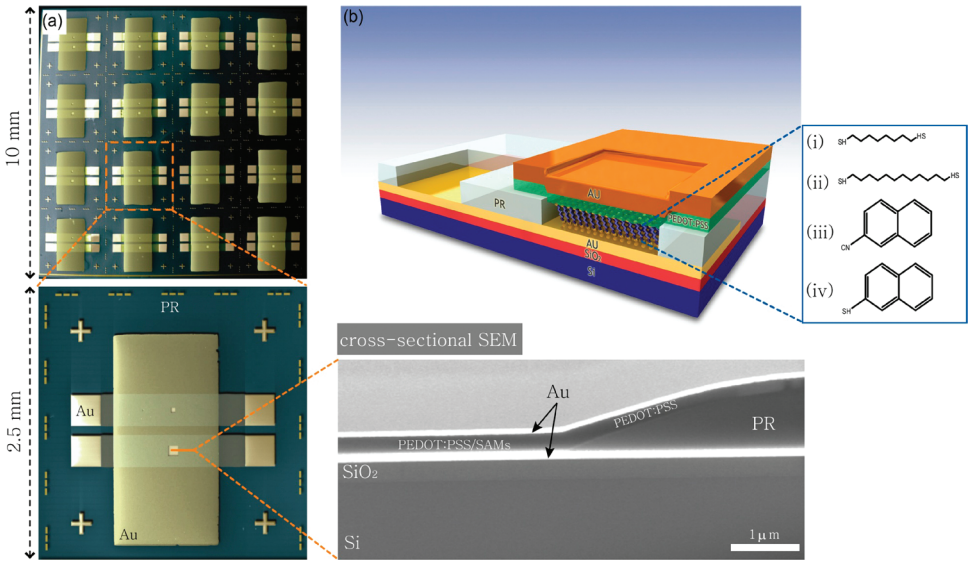

Figure 1. (a) SEM images of the fabricated molecular devices with microscale junctions. The junctions are square-shaped with side lengths of 40 and 90 μm. The cross-sectional SEM image of a molecular device is also shown. (b) Schematic view of a molecular device. Four types of molecules are shown with various chemical structures, including (i) DC8, (ii) DC12, (iii) Naph-NC, and (iv) Naph-SH.

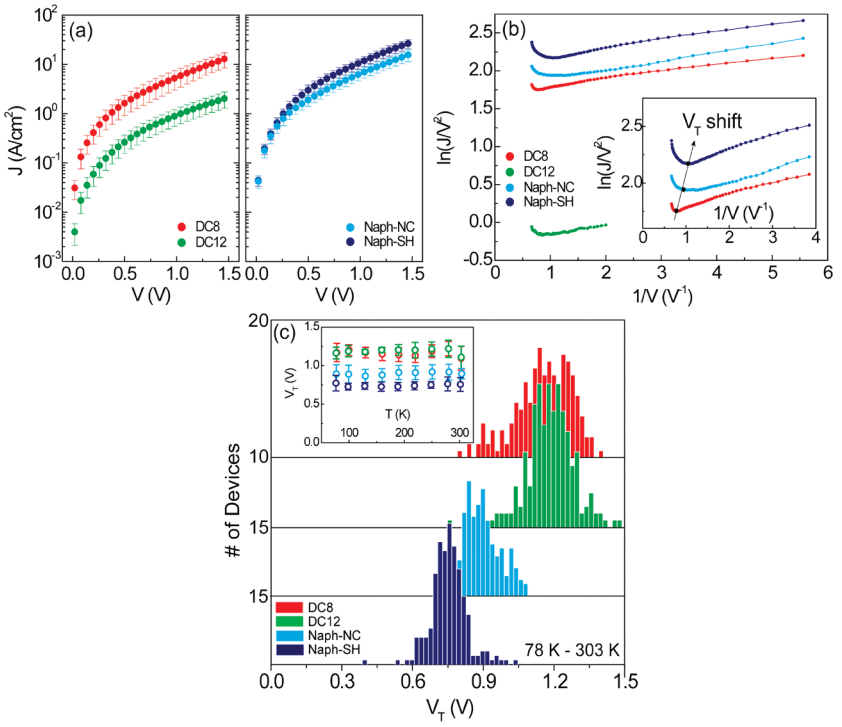

Figure 2. (a) Statistical $J-V$ data for all DC8, DC12, Naph-NC, and Naph-SH molecular devices measured at 303 K. (b) $\ln(J/V^2)-1/V$ plots for molecular junctions at 303 K. Inset shows a zoomed-in plot near V_T for DC8, Naph-NC, and the Naph-SH junction. (c) Histograms of V_T data points for the DC8, DC12, Naph-NC, and Naph-SH molecular devices at 78−303 K. The insets show V_T versus T plots for the DC8, DC12, Naph-NC, and Naph-SH molecular devices.

the top metal and the SAMs of the molecules. (See the cross-sectional SEM image in Figure 1a.)[19] We used four different molecules in our study, which can be distinguished according to their molecular backbone structures (i.e., alkyl-based vs oligoacene-based), the different lengths of the molecules, and the different metal−molecule contacts (i.e., Au-S vs Au-CN). Specifically, octanedithiol ((i) DC8) and dodecanedithiol ((ii) DC12) were used for alkanedithiols, and naphthalene-isocyanide ((iii) Naph-NC) and naphthalene-thiol ((iv) Naph-SH) were used for oligoacene-based molecules, as shown in Figure 1b. The details of molecular device fabrication are explained in the Experimental Section.

dx.doi.org/10.1021/jp204340w |J. Phys. Chem. C 2011, 115, 17979–17985

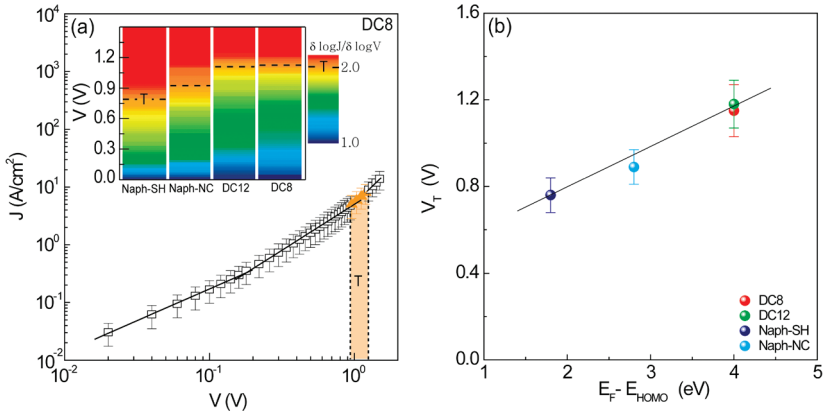

Figure 3. (a) Log−log plot of $J-V$ curves measured from 55 devices of alkyl-based molecules at 303 K. The orange region (marked as T) corresponds to $\delta\log(J)/\delta\log(V) \approx 2$, which is the minimum point appearing in the F−N plot. The inset shows the contour map of a differential $\log(J)-\log(V)$ plot as a function of V for different molecules. The dotted line in T corresponds to the minimum point (transition voltage V_T) in the F−N plot. (b) Experimental V_T values as a function of $E_F - E_{HOMO}$ for four molecular systems. The $E_F - E_{HOMO}$ values were obtained from the literature.[10,20,26]

We fabricated and characterized a number of molecular devices (~300 devices) to analyze the molecular electronic properties statistically. Figure 2a shows the statistical current density−voltage ($J-V$) data measured for four different molecular types at a temperature of 303 K. The error bars were calculated from the corresponding log-standard deviation of the individual devices for a total of ~300 devices. It can be seen that the $J-V$ characteristics depend on the molecular length (i.e., DC8 vs DC12) and the metal−molecule contacts (i.e., Naph-NC vs Naph-SH). The conductance of DC8 is higher than that of DC12 because of the length dependence of the tunneling conductance.[5,19] The difference in conductance between the Naph-SH and Naph-NC junctions can be explained by the metal−molecule contact properties of Au-S versus Au-CN. In fact, the Au-CN contact in molecular junctions is known to be more resistive than Au-S,[20] which indicates the presence of a higher tunneling barrier at the contact for isocynide (CN)-linked molecules. Figure 2b shows representative $\ln(J/V^2)-1/V$ plots (F−N plots) from the four types of molecular junctions measured at 303 K. The points (i.e., $\delta(\ln(J/V^2))/\delta(1/V) = 0$) in the curves are the minimum points (i.e., transition voltage V_T) in the F−N plot. A zoomed-in plot near the V_T for DC8, Naph-NC, and Naph-SH junction is shown in the inset of Figure 2b. Figure 2c shows the statistical histograms of V_T values (total 883 data) for the four types of molecular junctions determined from $I-V$ data measured at different temperatures ranging from 78 to 303 K. As previously mentioned, it is important to perform temperature-variable electrical characterizations to investigate charge conduction mechanisms. On the basis of the temperature-independent V_T characteristics (inset of Figure 2c), we can conclude that the conduction mechanism for the molecular junctions in this study was tunneling. Interestingly, V_T did not depend on the length of alkyl molecules based on our statistical analysis, which is in good agreement with previous experimental and theoretical results.[7,10,21] Note that the $J-V$ characteristics for our molecular junctions exhibited symmetric tunneling behavior in terms of the bias polarity. (See Figure S4 in the Supporting Information.) Furthermore, we did not observe a significant difference in the transition voltages between positive and negative bias regions for our molecular junctions.

The molecular orbital dependence of V_T can be further analyzed in terms of the slope of a log−log plot of $J-V$ characteristics.[12,22] Figure 3a shows a statistical $\log(J)-\log(V)$ plot for 55 DC8 molecular junctions measured at 303 K. It is important to note that near V_T, $\delta(\ln(J/V^2))/\delta(1/V)$ approaches zero because of the change in slope (Figure 2b), which corresponds to $\delta\log(J)/\delta\log(V) \approx 2$. (See the orange region in Figure 3a.) We marked the transition by T on the orange-colored TVS region corresponding to $\delta\log(J)/\delta\log(V) \approx 2$ in the $\log(J)-\log(V)$ plot, as shown in Figure 3a. The slopes of the $\log(J)-\log(V)$ plot for the four types of molecular junctions can be clearly displayed in the contour map of $\delta\log(J)/\delta\log(V)$ plots, as shown in the inset of Figure 3a. Note that the slope of the $\log(J)-\log(V)$ plot of molecular junctions sequentially changes from the blue- to the red-colored regions. The sequential change of the slope originates from the gradual increase in the molecular conductance ($\delta I/\delta V$) until the frontier orbital levels and the Fermi energy level of the electrodes match.[23−25] Figure 3b shows that V_T depends linearly on the energy offset $E_F - E_{HOMO}$ (in the case of a hole-type transport) for molecular junctions. Kim et al. reported that the E_{HOMO} value of oligoacene-SH series lies closer to E_F (Au) than that of the oligoacene-NC series by 0.7 to 1.3 eV based on ultraviolet photoelectron spectroscopy (UPS).[20] They suggested that the different offset $E_F - E_{HOMO}$ between the −S and −NC series is the reason for the difference in contact resistance (or junction resistance) between the oligoacene-SH and the oligoacene−NC molecules. The smaller offset observed for the oligoacene−SH molecule should produce more effective coupling between states in the metal and the HOMO level of the molecules, thereby reducing the effective barrier for tunneling at the contact. This result may suggest HOMO-mediated tunneling (i.e., p-type-like) transport. We also confirmed that the E_{HOMO} value of oligoacene-NC molecular series was closer to the E_F of the electrodes than the E_{LUMO} value according to a density functional theory (DFT) calculation. (See Table S1 in the Supporting Information.) In this regard, we suggest that the HOMO level dominates the transport (i.e., $E_F - E_{HOMO} < E_{LUMO} - E_F$) for oligoacene-based molecules in our study. The $E_F - E_{HOMO}$ values for the molecular systems used in our study are obtained from the literature,[10,20,26] as summarized in Table 1.

To better understand the physics behind V_T and the transport regime change in molecular junctions, we employed an extended coherent molecular transport model[10] that accounts for both of the frontier molecular orbital energy levels (i.e., E_{HOMO} and E_{LUMO}) with different coupling strengths to the electrodes.[18]

Table 1. Summary of Transport Parameters for Molecular Junctions[a]

molecular materials	$E_F - E_{HOMO}$ (eV)	exp. V_T (V) at 303 K	extended molecular coherent model cal. V_T $\eta = 1/2$)
$HS[CH_2]_NSH$	4[10,26]	1.09 ± 0.16 (for $N = 8$)	4.60 (for $6 < N < 14$)
		1.10 ± 0.15 (for $N = 12$)	
Naph-NC	2.8[20]	0.89 ± 0.07	3.22
Naph-SH	1.8[20]	0.77 ± 0.09	2.07

[a] $E_F - E_{HOMO}$ values for the molecular systems used in this study were obtained from the literature.[10,20,26]

This means that we considered both the contributions of tunneling electrons and holes near the frontier molecular orbital energy levels (i.e., LUMO and HOMO) and the asymmetric coupling effect. The $I-V$ characteristics were calculated from the Landauer formalism under the approximation that the entire potential drop occurs at the metal−molecule interface[8,10,11,18,27,28]

$$I(V) = \frac{2e}{h}\int_{-\infty}^{\infty} T(E)[f_1(E,V) - f_2(E,V)]\,dE \quad (1)$$

where $f_{1,2}(E,V) = (\exp((E - \mu_{1,2})/k_BT + 1)^{-1}$ is the Fermi distribution function for temperature T, the chemical potential is $\mu_1 = eV/2$ for the left contact and $\mu_2 = -eV/2$ for the right contact, k_B is the Boltzmann constant, and $T(E)$ is the Lorentzian-based transmission function that depends explicitly on energy E that peaks near the molecular orbital levels.[10,27−29] Furthermore, because the molecules used in our study are strongly coupled only to the Au bottom electrode, the molecular orbital level is likely to follow the chemical potential of the Au bottom contact.[30] Therefore, when a finite voltage is applied, these Lorentzian peaks will follow the chemical potential of the Au bottom electrode due to the stronger coupling to this electrode.[18,30] With this consideration in mind, we assumed that the position of the Lorentzian peaks (E_{HOMO} and E_{LUMO}) shifts from their original position by the degree of $(1/2 - \eta) \times V$ when a finite voltage is applied.[18] Note that for the simplicity in the modeling we have assumed that the asymmetry in the electronic coupling is similar to the asymmetry in the voltage drop. Although the asymmetry in the voltage drop (i.e., asymmetry in the electrostatic potential drop) may not be exactly the same as the asymmetry in the electronic coupling (e.g., strong chemisorbed coupling, or poor physisorbed coupling), these two concepts of asymmetry are related each other. For example, the voltage drop across poor electronic coupling would be larger than that across strong electronic coupling. So, it would be a reasonable assumption that the asymmetry in the electronic coupling is similar to the asymmetry in the voltage drop. With this assumption, the voltage-dependent transmission function $T(E,V)$ can be expressed as follows.

$$T(E,V) = \frac{1}{\frac{1}{4\eta(1-\eta)} + \left(\frac{E - (E_{HOMO} + (1/2-\eta)\times V)}{E_F - (E_{HOMO} + (1/2-\eta)\times V)}\right)^2 \exp(\beta_{HOMO}d)} + \frac{1}{\frac{1}{4\eta(1-\eta)} + \left(\frac{E - (E_{LUMO} + (1/2-\eta)\times V)}{E_F - (E_{LUMO} + (1/2-\eta)\times V)}\right)^2 \exp(\beta_{LUMO}d)} \quad (2)$$

The details of the calculated $T(E,V)$ are explained in the Supporting Information. In the case of symmetric coupling with

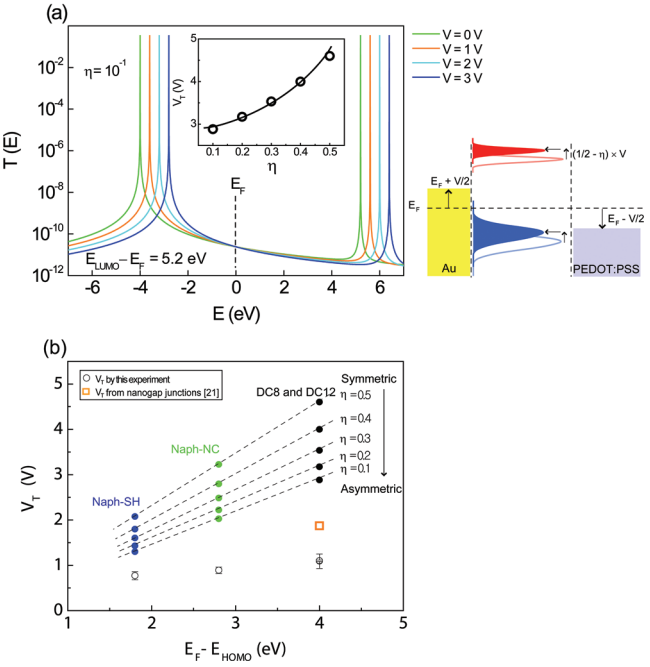

Figure 4. (a) $T(E,V)$ for $N = 6$ in alkanedithiol junctions considering both E_{HOMO} (−4 eV) and E_{LUMO} (5.2 eV) under the condition of asymmetric coupling ($\eta = 10^{-1}$). A schematic of the energy band diagram illustrates how the molecular orbital levels move under finite voltage and asymmetric coupling. The inset shows the $V_T-\eta$ plot for $N = 6$ in the alkanedithiol molecular junction. (b) V_T values calculated by the extended coherent molecular model considering both HOMO and LUMO levels under the condition asymmetric coupling as a function of $E_F - E_{HOMO}$ for alkanedithiols, Naph-NC, and Naph-SH molecular junctions at room temperature. The data used to derive the open black circles and the open orange square have been obtained from the PEDOT:PSS devices in this study and nanogap junctions in our previous study,[21] respectively.

$\eta = 1/2$, the positions of the Lorentzian peaks do not change from the original positions (i.e., E_{HOMO} and E_{LUMO}), regardless of the applied voltage. However, for a given degree of asymmetry η ($0 < \eta < 1/2$), the Lorentzian peaks shift relative to the E_F value of the electrode when a positive voltage is applied. In fact, this assumption is valid for the asymmetric molecular junctions with one chemisorbed contact (e.g., Au-S and Au-CN) and one physisorbed contact (e.g., molecule/PEDOT:PSS).

Figure 4a shows the calculated $T(E,V)$ for $N = 6$ in alkanedithiol junctions considering both the HOMO (−4 eV) and LUMO (5.2 eV) levels under the asymmetric coupling condition ($\eta = 10^{-1}$). As shown in Figure 4a, the Lorentzian peaks shifted upward in energy when a voltage was applied. This upward shift of $T(E,V)$ can lead to a reduction in the V_T corresponding to the inflection feature in the F−N plot when the electronic coupling is

more asymmetric ($\eta \rightarrow 0$). (See the inset of Figure 4a.) We also calculated the $T(E,V)$ and V_T values for different numbers of conjugation (N) in an oligoacene-based junction by considering both the HOMO and LUMO frontier molecular orbital levels under symmetric or asymmetric coupling conditions. (See Figure S7 in the Supporting Information.). Figure 4b shows the calculated V_T values for various molecular junctions as a function of $E_F - E_{HOMO}$ using eq 2. The TVS characteristics indicate that the V_T positions of molecular junctions are determined by both the energy offsets ($E_F - E_{HOMO}$) and the degree of asymmetric coupling (η). When the asymmetric factor η approaches zero (i.e., more asymmetric) and when the energy offset ($E_F - E_{HOMO}$, in the case of a hole-type transport) is smaller, V_T is reduced. This linear dependence of TVS on the energy offsets ($E_F - E_{HOMO}$) is in agreement with our experimental results. Furthermore, we can recognize from the V_T result in Figure S6 in the Supporting Information that the linear dependence of V_T versus $E_F - E_{HOMO}$ is maintained, regardless of the LUMO level position in the case of a hole-dominant transport, as $E_F - E_{HOMO} < E_{LUMO} - E_F$.

By considering the asymmetric factor η on V_T, we can explain the difference of the experimental V_T according to the PEDOT:PSS-based junction and a nanogap system. In the case of the alkanedithiol molecule, we observed that the V_T observed in PEDOT:PSS-based junctions was found to be smaller than that observed in the nanogap junctions.[21] This difference can be explained by the following argument; the PEDOT:PSS-based junction system has a relatively more asymmetric contact coupling due to the poor top contact of S/PEDOT:PSS as compared with the chemisorbed bottom contact property of Au-S.[31,32] In the alkanedithiol junction in the nanogap junction system, however, both chemisorbed contact groups lie at both sides of Au electrodes. Therefore, the V_T value is larger because of the relatively more symmetric junction coupling in the nanogap junctions. This result indicates that it is important to consider the asymmetric coupling for a more comprehensive interpretation of V_T in a molecular junction system. Nevertheless, note that there is a significant discrepancy in the magnitude of V_T between the experimental and the calculated values in Figure 4b, which is often ascribed to the tunneling barrier lowering effects such as many-electron interactions.[33] These many-electron interactions can lead to shifting the transmission function $T(E)$ with respect to the E_F value of the electrode[33−36] and narrowing the width of Lorentzian peaks under the weak coupling limit.[37,38] Furthermore, the geometric feature of the molecules on the electrodes and their contact sites affect the shape of the transmission function $T(E)$.[33,38,39] We noticed that a more appropriate modeling of molecular junction systems would include the effect of electron correlation effect (the many-electron interaction) and the exact geometry of the molecules on the electrodes. Note that the sequential change in the slope of the $\log(I)-\log(V)$ plot in the molecular junctions can be also described by the extended coherent molecular model (Figure S8 in the Supporting Information).

CONCLUSIONS

In summary, we both experimentally and theoretically investigated the TVS and the sequential change in the slope of the $\log(I)-\log(V)$ plot for selected molecular junctions that are distinguished by molecular structure (i.e., alkyl- and oligoacene-based), molecular length, and functional group (i.e., −NC and −SH). The temperature-independent, asymmetric-coupling-, molecular-length-, and orbital-dependent TVS and the sequential change in the slope of the $\log(I)-\log(V)$ plot were demonstrated experimentally. The observed features were explained well by the extended coherent model by considering both the HOMO and LUMO levels of molecules and the asymmetry of the coupling to the electrodes. This study extends current understandings of both charge transport in molecular junctions as well as TVS characteristics.

ASSOCIATED CONTENT

Supporting Information. Additional information is available on the process flow of the molecular device, temperature-variable $J-V$ characteristics and Log−log plots of the statistical $J-V$ data, theoretical models (i.e., the Coherent molecular model considering frontier molecular orbitals and asymmetric coupling effect); and molecular orbital levels for oligoacene-NC based on DFT. This material is available free of charge via the Internet at http://pubs.acs.org.

AUTHOR INFORMATION

Corresponding Author
*E-mail: takheelee@gmail.com.

Present Addresses
⊥Department of Physics and Astronomy, Seoul National University, Seoul 151−747, Korea.

ACKNOWLEDGMENT

This work was supported by the National Research Laboratory program; a Korean National Core Research Center grant; the World Class University program of the Korean Ministry of Education, Science, and Technology; and the Program for Integrated Molecular Systems at the Gwangju Institute of Science and Technology.

REFERENCES

(1) Joachim, C.; Gimzewski, J. K.; Aviram, A. Electronics using hybrid-molecular and mono-molecular devices. *Nature* **2000**, *408*, 541–548.

(2) Nitzan, A.; Ratner, M. A. Electron transport in molecular wire junctions. *Science* **2003**, *300*, 1384–1389.

(3) Song, H.; Kim, Y.; Jang, Y. H.; Jeong, H.; Reed, M. A.; Lee, T. Observation of molecular orbital gating. *Nature* **2009**, *462*, 1039–1043.

(4) Ohara, M.; Kim, Y.; Yanagisawa, S.; Morikawa, Y.; Kawai, M. Role of molecular orbitals near the Fermi level in the excitation of vibrational modes of a single molecule at a scanning tunneling microscope junction. *Phys. Rev. Lett.* **2008**, *100*, 136104.

(5) Salomon, A.; Cahen, D.; Lindsay, S.; Tomfohr, J.; Engelkes, V. B.; Frisbie, C. D. Comparison of electronic transport measurements on organic molecules. *Adv. Mater.* **2003**, *15*, 1881–1890.

(6) Beebe, J. M.; Kim, B.; Gadzuk, J. W.; Frisbie, C. D.; Kushmerick, J. G. Transition from direct tunneling to field emission in metal−molecule−metal junctions Junctions. *Phys. Rev. Lett.* **2006**, *97*, 026801.

(7) Beebe, J. M.; Kim, B.; Frisbie, C. D.; Kushmerick, J. G. Measuring relative barrier heights in molecular electronic junctions with transition voltage spectroscopy. *ACS Nano* **2008**, *2*, 827–832.

(8) Kushmerick, J. G.; Holt, D. B.; Yang, J. C.; Naciri, J.; Moore, M. H.; Shashidhar, R. Metal-molecule contacts and charge transport across monomolecular layers: measurement and theory. *Phys. Rev. Lett.* **2002**, *89*, 086802.

(9) Chen, J.; Calvet, L. C.; Reed, M. A.; Carr, D. W.; Grubisha, D. S.; Bennett, D. W. Electronic transport through metal-1,4-phenylene diisocyanide-metal junctions. *Chem. Phys. Lett.* **1999**, *313*, 741–748.

(10) Huisman, E. H.; Guédon, C. M.; van Wees, B. J.; van der Molen, S. J. Interpretation of transition voltage spectroscopy. *Nano Lett* **2009**, *9*, 3909–3913.

(11) Araidai, M.; Tsukada, M. Theoretical calculations of electron transport in molecular junctions: Inflection behavior in Fowler-Nordheim plot and its origin. *Phys. Rev. B* **2010**, *81*, 235114.

(12) Choi, S. H.; Kim, B.; Frisbie, C. D. Electrical resistance of long conjugated molecular wires. *Science* **2008**, *320*, 1482–1486.

(13) Wang, G.; Kim, T.-W.; Jo, G.; Lee, T. Enhancement of field emission transport by molecular tilt configuration in metal−molecule−metal junctions junctions. *J. Am. Chem. Soc.* **2009**, *131*, 5980–5985.

(14) Smaali, K.; Lenfant, S.; Karpe, S.; Ocafrain, M.; Blanchard, P.; Deresmes, D.; Godey, S.; Rochefort, A.; Roncali, J.; Vuillaume, D. High on-off conductance switching ratio in optically-driven self-assembled conjugated molecular systems. *ACS Nano* **2010**, *4*, 2411–2421.

(15) Tan, A.; Sadat, S.; Reddy, P. Measurement of thermopower and current-voltage characteristics of molecular junctions to identify orbital alignment. *Appl. Phys. Lett.* **2010**, *96*, 013110.

(16) Choe, M.; Jo, G.; Maeng, J.; Hong, W.-K.; Jo, M.; Wang, G.; Park, W.; Lee, B. H.; Hwang, H.; Lee, T. Electrical properties of ZnO nanowire field effect transistors with varying high-*k* Al^2O^3 dielectric thickness. *J. Appl. Phys.* **2010**, *107*, 034504.

(17) Simmons, J. G. Generalized formula for the electric tunnel effect between similar electrodes separated by a thin insulating film. *J. Appl. Phys.* **1963**, *34*, 1793.

(18) Chen, J.; Markussen, T.; Thygesen, K. S. Quantifying transition voltage spectroscopy of molecular junctions: ab initio calculations. *Phys. Rev. B* **2010**, *82*, 121412.

(19) Akkerman, H. B.; Blom, P. W. M.; de Leeuw, D. M.; de Boer, B. Towards molecular electronics with large-area molecular junctions. *Nature* **2006**, *441*, 69–72.

(20) Kim, B.; Beebe, J. M.; Jun, Y.; Zhu, X. Y.; Frisbie, C. D. Correlation between HOMO alignment and contact resistance in molecular junctions: aromatic thiols versus aromatic isocyanides. *J. Am. Chem. Soc.* **2006**, *128*, 4970–4971.

(21) Song, H.; Kim, Y.; Jeong, H.; Reed, M. A.; Lee, T. Coherent tunneling transport in molecular junctions. *J. Phys. Chem. C* **2010**, *114*, 20431–20435.

(22) Bâldea, I. Revealing molecular orbital gating by transition voltage spectroscopy. *Chem. Phys.* **2010**, *377*, 15–20.

(23) Lötscher, E.; Weber, H. B.; Riel, H. Statistical approach to investigating transport through single molecules. *Phys. Rev. Lett.* **2007**, *98*, 176807.

(24) Lötscher, E.; Elbing, M.; Tschudy, M.; von, Hänisch., C.; Weber, H. B.; Mayor, M.; Riel, H. Charge transport through molecular rods with reduced pi-conjugation. *Chem. Phys. Chem.* **2008**, *9*, 2252–2258.

(25) Hong, S.; Reifenberger, R.; Tian, W.; Datta, S.; Henderson, J. I.; Kubiak, C. P. Molecular conductance spectroscopy of conjugated, phenyl-based molecules on Au(111): the effect of end groups on molecular conduction. *Superlattices Microstruct.* **2000**, *28*, 289–303.

(26) Akkerman, H. B.; Naber, R. C. G.; Jongbloed, B.; van Hal, P. A.; Blom, P. W. M.; de Leeuw, D. M.; de Boer, B. Electron tunneling through alkanedithiol self-assembled monolayers in large-area molecular junctions. *Proc Natl Acad Sci USA* **2007**, *104*, 11161–11166.

(27) Datta, S. *Quantum Transport: Atom To Transistor*; Cambridge University Press: Cambridge, U.K., 2005.

(28) Paulsson, M.; Datta, S. Thermoelectric effect in molecular electronics. *Phys. Rev. B* **2003**, *67*, 241403.

(29) Malen, J. A.; Doak, P.; Baheti, K.; Tilley, T. D.; Segalman, R. A.; Majumdar, A. Identifying the length dependence of orbital alignment and contact coupling in molecular heterojunctions. *Nano Lett.* **2009**, *9*, 1164–1169.

(30) Peng, G.; Strange, M.; Thygesen, K. S.; Mavrikakis, M. Conductance of conjugated molecular wires: length dependence, anchoring groups, and band alignment. *J. Phys. Chem. C* **2009**, *113*, 20967–20973.

(31) Wang, G.; Kim, Y.; Choe, M.; Kim, T.-W.; Lee, T. A new approach for molecular electronic junctions with a multilayer graphene electrode. *Adv. Mater.* **2010**, *23*, 755–760.

(32) Wang, G.; Yoo, H.; Na, S.-I.; Kim, T.-W.; Cho, B.; Kim, D.-Y.; Lee, T. Electrical conduction through self-assembled monolayers in molecular junctions: Au/molecules/Au versus Au/molecule/PEDOT:PSS/Au. *Thin Solid Films* **2009**, *518*, 824–828.

(33) Quek, S. Y.; Venkataraman, L.; Choi, H. J.; Louie, S. G.; Hybertsen, M. S.; Neaton, J. B. Amine-gold linked single-molecule circuits: experiment and theory. *Nano Lett.* **2007**, *7*, 3477–3482.

(34) Neaton, J. B.; Hybertsen, M. S.; Louie, S. G. Renormalization of molecular electronic levels at metal-molecule interfaces. *Phys. Rev. Lett.* **2006**, *97*, 216405.

(35) Darancet, P.; Ferretti, A.; Mayou, D.; Olevano, V. Ab initio GW electron-electron interaction effects in quantum transport. *Phys. Rev. B* **2007**, *75*, 075102.

(36) Koentopp, M.; Burke, K.; Evers, F. Zero-bias molecular electronics: exchange-correlation corrections to Landauer's formula. *Phys. Rev. B* **2006**, *73*, 121403.

(37) Ferretti, A.; Calzolari, A.; Di Felice, R.; Manghi, F.; Caldas, M. J.; Nardelli, M. B.; Molinari, E. First-principles theory of correlated transport through nanojunctions. *Phys. Rev. Lett.* **2005**, *94*, 116802.

(38) Thygesen, K. S.; Rubio, A. Renormalization of molecular quasiparticle levels at metal-molecule interfaces: trends across binding regimes. *Phys. Rev. Lett.* **2009**, *102*, 046802.

(39) Li, Z.; Kosov, D. S. Nature of well-defined conductance of amine-anchored molecular junctions: density functional calculations. *Phys. Rev. B* **2007**, *76*, 035415.